


Article

# Topology Perception and Relative Positioning of UAV Swarm Formation Based on Low-Rank Optimization

Chengliang Di and Xiaozhou Guo \* 

The 54th Research Institute of China Electronics Technology Group Corporation, Shijiazhuang 050000, China

\* Correspondence: xiaozhouguo@foxmail.com

**Abstract:** In a satellite-denied environment, a swarm of drones is capable of achieving relative positioning and navigation by leveraging the high-precision ranging capabilities of the inter-drone data link. However, because of factors such as high drone mobility, complex and time-varying channel environments, electromagnetic interference, and poor communication link quality, distance errors and even missing distance values between some nodes are inevitable. To address these issues, this paper proposes a low-rank optimization algorithm based on the eigenvalue scaling of the distance matrix. By gradually limiting the eigenvalues of the observed distance matrix, the algorithm reduces the rank of the matrix, bringing the observed distance matrix closer to the true value without errors or missing data. This process filters out distance errors, estimates and completes missing distance elements, and ensures high-precision calculations for subsequent topology perception and relative positioning. Simulation experiments demonstrate that the algorithm exhibits significant error filtering and missing element completion capabilities. Using the F-norm metric to measure the relative deviation from the true value, the algorithm can optimize the relative deviation of the observed distance matrix from 11.18% to 0.25%. Simultaneously, it reduces the relative positioning error from 518.05 m to 35.24 m, achieving robust topology perception and relative positioning for the drone swarm formation.

**Keywords:** satellite-denied; UAV swarm; topology perception; relative positioning



**Citation:** Di, C.; Guo, X. Topology Perception and Relative Positioning of UAV Swarm Formation Based on Low-Rank Optimization. *Aerospace* **2024**, *11*, 466. <https://doi.org/10.3390/aerospace11060466>

Academic Editor: Wojciech Skarka

Received: 15 March 2024

Revised: 5 June 2024

Accepted: 5 June 2024

Published: 11 June 2024



**Copyright:** © 2024 by the authors. Licensee MDPI, Basel, Switzerland. This article is an open access article distributed under the terms and conditions of the Creative Commons Attribution (CC BY) license (<https://creativecommons.org/licenses/by/4.0/>).

## 1. Introduction

Unmanned aerial vehicles (UAVs), with their flexibility, efficiency, and relatively low cost, have demonstrated significant application potential in military fields, such as aerial reconnaissance [1], battlefield observation [2], damage assessment [3], battlefield suppression, ground attack, missile interception [4], aerial combat, and communication relay [5]. With the development of communication and artificial intelligence technologies, the concept of UAV swarm formation has gradually emerged. Forming a swarm intelligence system through data links enables multiple UAVs to achieve higher collective combat effectiveness [6]. UAV swarm formations can simultaneously reconnoiter and monitor vast areas and rapidly perceive and assess battlefield situations through information sharing and collaborative processing mechanisms within the swarm [7]. Additionally, the swarm can flexibly adjust its attack strategies based on battlefield conditions, enabling simultaneous or continuous distributed strikes against multiple targets [8]. Furthermore, UAV swarm formations possess powerful electronic countermeasures, capable of disrupting and paralyzing enemy communication and radar systems through coordinated jamming and deception [9,10].

The effectiveness of UAV swarm formation operations relies on the swarm's topology control [11] and node positioning capabilities. In open battlefield environments, satellite positioning systems, such as GPS [12], Beidou [13], and Galileo [14], can provide stable and precise positioning services. However, under conditions where satellite navigation services are denied, topology perception and positioning must rely solely on the swarm's relative

ranging and angle measurement information for calculation and control. Relative positioning techniques can utilize the distance information measured by the inter-drone data link to calculate the relative positions of UAVs within the swarm and perform topology perception calculations [15,16]. Once the absolute geographical coordinates of individual nodes are obtained, the absolute geographical coordinates of all nodes can be determined [17]. However, in complex electromagnetic battlefield environments, radio signals may be affected by factors such as high-intensity interference [18], channel attenuation [19], multipath effects, and Doppler effects [20], leading to significant errors in distance values and even unobtainable distance values between some nodes. In this scenario, the obtained distance matrix of the swarm deviates significantly from the actual distance matrix. If a relative positioning calculation is performed directly, it leads to significant positioning errors, which may prevent the drones from successfully completing assigned tasks.

To address this issue, this paper first analyzes the low-rank characteristics of the distance matrix in UAV swarm formations. Subsequently, based on these low-rank characteristics, an optimization method for the observed distance matrix is proposed. This method utilizes a low-rank optimization algorithm based on eigenvalue scaling of the distance matrix. By gradually limiting the eigenvalues of the observed distance matrix, the rank of the matrix is reduced, thereby filtering out distance errors and estimating and completing missing values. Relevant simulation experiments are conducted to verify the effectiveness of the proposed method.

## 2. Related Work

In the implementation of relative positioning technology in denied environments, some researchers have attempted to equip a single platform with multiple heterogeneous sensors, such as cameras [21], barometers [22], inertial navigation systems [23,24], and range and angle measurement devices [25,26]. These sensors, combined with multi-sensor data fusion algorithms [27,28], aim to achieve positioning. However, multi-sensor systems inevitably affect the flexibility of drones and are not suitable for large-scale, low-cost swarm systems [29]. Other researchers have coupled data links [30] with inertial navigation systems using Kalman filtering algorithms [31] to achieve high output rate and high-precision positioning. However, inertial navigation systems require a long initial alignment time and need to be associated with absolute geographical coordinates for position calculations, limiting their application scenarios [32]. Methods such as leader–follower [33,34] positioning and Link-16 [35] relative positioning are centralized positioning approaches. Their positioning accuracy depends on the spatial position sensing capabilities of the central node [36]. If the central node is damaged, all other nodes lose their positioning capabilities, resulting in poor overall battlefield survivability for the swarm formation [37]. Relative positioning techniques based on data links rely on the high-precision ranging capabilities of the unmanned system's data link to obtain pseudo-range information between nodes and complete the calculation of their relative configurations. When the absolute geographical positions of some nodes are obtained through a measurement and control system or inertial navigation, visual navigation, and other means, the absolute geographical positions of all nodes can be recovered [38]. This technology enables the integration of communication and navigation positioning without adding additional hardware [39], offering strong resilience [40] and good positioning accuracy [41] to support flexible combat missions.

Overall, for multi-node, low-cost, lightweight drone swarm formations, it is difficult to configure multi-source sensors because of constraints such as power consumption and flexibility. For topology control under satellite-denied conditions, relying on the relative ranging assistance function of the swarm's data link to achieve topology perception and relative positioning is a reasonable and suitable technical approach. However, there is currently limited research and related work in this field. Moreover, existing research has not optimized the distance matrix, resulting in relatively large positioning errors in cases of large distance errors or missing distance values. This work utilizes the low-rank property

of the distance matrix to enhance the robustness of the positioning system and ensures the reliability of relative positioning for unmanned swarms under satellite denial.

### 3. The Low-Rank Property of Distance Matrices in Swarm Formation

We first analyze the rank of the distance matrix for drone swarm formation. In a swarm formation consisting of  $N$  nodes, let  $r_i$  represent the position vector of the  $i$ th drone node. Then, the coordinate matrix  $R_{3 \times N}$  is defined as follows:

$$R = [r_1, r_2, \dots, r_N] \tag{1}$$

where  $N$  represents the number of drone swarm nodes and 3 represents the coordinate dimension. Define drone swarm formation distance matrix as  $P = [p_{ij}]_{N \times N}$ , where  $p_{ij}$  represents the Euclidean distance between the  $i$ -th node and the  $j$ -th node, as shown in Figure 1.

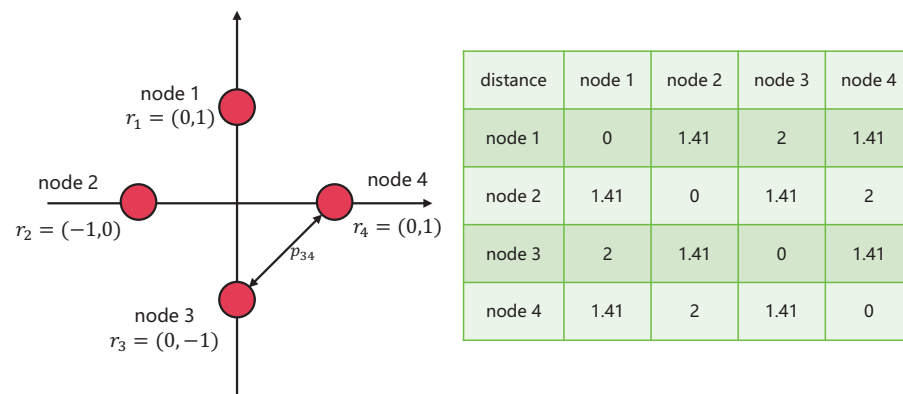


Figure 1. Schematic diagram of distance matrix for drone swarm formation.

The inner product matrix for clustering formation is defined as  $Q = [q_{ij}]_{N \times N}$ , where  $q_{ij} = r_i \cdot r_j^T$ , which indicates the inner product of position vectors  $r_i$  and  $r_j$ . It can be easily known that there is a computational relationship between  $P$  and  $Q$ :

$$P = \mathbf{diag}(Q) \cdot \mathbf{1}^T + \mathbf{1} \cdot \mathbf{diag}(Q) - 2Q \tag{2}$$

$\mathbf{diag}(Q)$  represents an  $N$ -dimensional column vector composed of the diagonal elements of  $Q$ , i.e.,

$$\mathbf{diag}(Q) = [Q_{11}, Q_{22}, \dots, Q_{NN}]^T \tag{3}$$

Similarly,  $\mathbf{1}$  represents an  $N$ -dimensional column vector with all elements being 1, i.e.,

$$\mathbf{1} = [1, 1, \dots, 1]^T \tag{4}$$

According to the basic properties of matrix rank, the rank of the distance matrix  $P$ ,  $\text{rank}(P)$ , satisfies the following inequality:

$$\text{rank}(P) \leq \text{rank}(\mathbf{diag}(Q) \cdot \mathbf{1}^T) + \text{rank}(\mathbf{1} \cdot \mathbf{diag}(Q)) + \text{rank}(-2Q) \tag{5}$$

For the first and second terms on the right side of the inequality, since the ranks of both the vector  $\mathbf{diag}(Q)$  and the vector  $\mathbf{1}$  are 1,

$$\text{rank}(\mathbf{diag}(Q) \cdot \mathbf{1}^T) + \text{rank}(\mathbf{1} \cdot \mathbf{diag}(Q)) \leq 2 \min \text{rank}(\mathbf{diag}(Q)), \text{rank}(\mathbf{1}^T) = 2 \tag{6}$$

For the third term on the right side of the inequality, since  $Q = X^T X$  and the rank of  $X$  is 2,

$$\text{rank}(-2Q) \leq \min \text{rank}(X^T), \text{rank}(X) = 3 \tag{7}$$

In summary, it can be concluded that  $\text{rank}(P) \leq 4$ . Since the number of nodes  $N$  in the drone formation is usually much larger than 4, i.e.,  $\text{rank}(P) \ll N$ , and the drone swarm formation distance matrix  $P$  can be regarded as a low-rank matrix.

The low-rank property suggests that there is a high linear correlation between the row or column vectors in the distance matrix  $P$ , and most rows or columns can be represented by linear combinations of other rows or columns, indicating that  $P$  itself contains relatively low information content. However, according to simulation results, because of distance errors and missing distance values during actual flights, the rank of the observed drone swarm formation distance matrix often jumps to  $N$ , no longer satisfying the low-rank property and containing a significantly larger amount of information. This increase in the rank suggests that the observed distance matrix contains significantly more information compared to  $P$ , and the amount of additional information is related to distance errors and missing values.

We consider reducing the rank of the observed distance matrix to eliminate information unrelated to the intrinsic values of distances, filtering out distance errors, filling missing distance values, and ultimately achieving high-precision approximation and reconstruction of the distance matrix.

#### 4. Eigenvalue Scaling-Based Low-Rank Optimization Algorithm for UAV Swarm Formation Distance Matrix

The eigenvalue scaling-based low-rank optimization algorithm (ESLO) utilizes norm approximation, regularization relaxation, and other methods to model the low-rank optimization problem of the UAV swarm formation distance matrix. It achieves numerical solutions for low-rank optimization by gradually scaling the eigenvalues of the matrix, thereby reducing the rank of the observed distance matrix, eliminating distance errors, and estimating missing distance elements simultaneously.

##### 4.1. Problem Modeling

Let  $O_{N \times N}$  denote the observed distance matrix during the actual flight of the unmanned aerial vehicle swarm formation. Let  $\omega$  represent the index set of all non-missing elements in the observed distance matrix  $O$ , i.e.,  $\omega \subset [n_1] \times [n_2]$  (where  $n_1 = 1, 2, \dots, N$  and  $n_2 = 1, 2, \dots, N$ ). Define the operator  $S(\cdot)$  as the projection operator, i.e.,

$$[S_\omega(X)]_{ij} = \begin{cases} X_{ij}, & (i, j) \in \omega \\ 0, & \text{otherwise} \end{cases} \quad (8)$$

The low-rank optimization problem for the observed distance matrix is formulated as

$$\begin{aligned} & \min \text{rank}(X) \\ & \text{s.t. } O_{ij} = [S_\omega(X)]_{ij}, \end{aligned} \quad (9)$$

where  $X$  represents the distance matrix to be optimized. Let  $\Omega$  denote the vector composed of the  $N$  eigenvalues of  $X$ :

$$\Omega = [\sigma_1, \sigma_2, \dots, \sigma_N]^T \quad (10)$$

where  $\sigma_i$  represents the  $i$ -th eigenvalue of  $X$ . The rank of  $X$  is equivalent to the  $L_0$  norm of the eigenvalue vector  $\Omega$ :

$$\text{rank}(X) = |\Omega|_{L_0} \quad (11)$$

Since solving the  $L_0$  norm of a vector is an NP-hard problem that cannot be solved in polynomial time, the nuclear norm is used as an approximation. The nuclear norm of the distance matrix  $X$  is defined as

$$|X|_* = \sum_{i=1}^N \sigma_i \quad (12)$$

Using the nuclear norm essentially replaces the  $L_0$  norm of the eigenvalue vector  $\Omega$  with the  $L_1$  norm, allowing the optimization problem to be solved in polynomial time. The optimization problem is then formulated as

$$\begin{aligned} \min |X|_* \\ \text{s.t. } O_{ij} = [S_\omega(X)]_{ij} \end{aligned} \quad (13)$$

To accelerate the convergence of the solution, regularization terms can be added. The low-rank optimization problem for the observed distance matrix of the UAV swarm formation is finally modeled as

$$\begin{aligned} \min \mu |X|_* + \frac{1}{2} |X|_F^2 \\ \text{s.t. } O_{ij} = [S_\omega(X)]_{ij}, \end{aligned} \quad (14)$$

where  $|\cdot|_F$  represents the Frobenius norm of the matrix, calculated as

$$|X|_F = \left( \sum_{i,j} x_{ij}^2 \right)^{\frac{1}{2}} \quad (15)$$

$\mu$  is a positive constant. Theory suggests that as  $\mu \rightarrow \infty$ , the optimal solution of problem 14 converges to that of problem 13.

#### 4.2. Problem Solving

To solve the low-rank optimization problem 14 of the observation distance matrix for the drone swarm formation, the Lagrange multiplier method is considered. Based on the optimization objective and constraints, the Lagrange function  $L(X, \lambda)$  is defined as

$$L(X, \lambda) = \mu |X|_* + \frac{1}{2} |X|_F^2 + \lambda ([S_\omega(X)]_{ij} - O_{ij}) \quad (16)$$

where  $\lambda$  represents the Lagrange multiplier. The optimal values  $X^*$  and  $\lambda^*$  satisfy the following condition:

$$X^*, \lambda^* = \sup_X \inf_\lambda L(X, \lambda) \quad (17)$$

To find the optimal values  $X^*$  and  $\lambda^*$ , an alternating iteration method can be used. Given  $\lambda^{(k)}$ ,  $X^{(k+1)}$  is obtained by satisfying the following condition:

$$\frac{\partial L(X, \lambda)}{\partial X} \Big|_{X^{(k+1)}, \lambda^{(k)}} = 0 \quad (18)$$

This equation can be solved by applying scaling to the eigenvalues of the matrix. Eigenvalue decomposition of  $X^{(k)}$  gives

$$X^{(k)} = V \begin{bmatrix} \gamma_1 & \dots & 0 \\ 0 & \dots & 0 \\ 0 & 0 & \gamma_N \end{bmatrix} V^T \quad (19)$$

where  $\gamma_i$  represents the  $i$ -th eigenvalue. By setting an eigenvalue scaling threshold  $\mu$ , eigenvalues less than  $\mu$  are scaled to 0, while eigenvalues greater than  $\mu$  are reduced by  $\mu$ . This scaling is achieved using the eigenvalue scaling function  $h(\cdot)$ :

$$h(\gamma_i) = \text{sgn}(\gamma_i) \cdot \max(\text{abs}(\gamma_i) - \mu, 0) \quad (20)$$

According to  $\gamma'_i = h(\gamma_i)$ ,  $X_{(k+1)}$  is computed as

$$X_{(k+1)} = V \begin{bmatrix} \gamma'_1 & \dots & 0 \\ 0 & \dots & 0 \\ 0 & 0 & \gamma'_N \end{bmatrix} V^T \tag{21}$$

Additionally,  $\lambda_{(k+1)}$  is updated using the following formula:

$$\lambda_{(k+1)} = \lambda_{(k)} + \epsilon \cdot S_\omega(O - X) \tag{22}$$

where  $\epsilon$  represents the iteration step. After completing the low-rank optimization of the actual observation distance matrix, the algorithm automatically filters out some observation distance errors and simultaneously estimates and recovers missing distance values. The effect is illustrated in Figure 2.

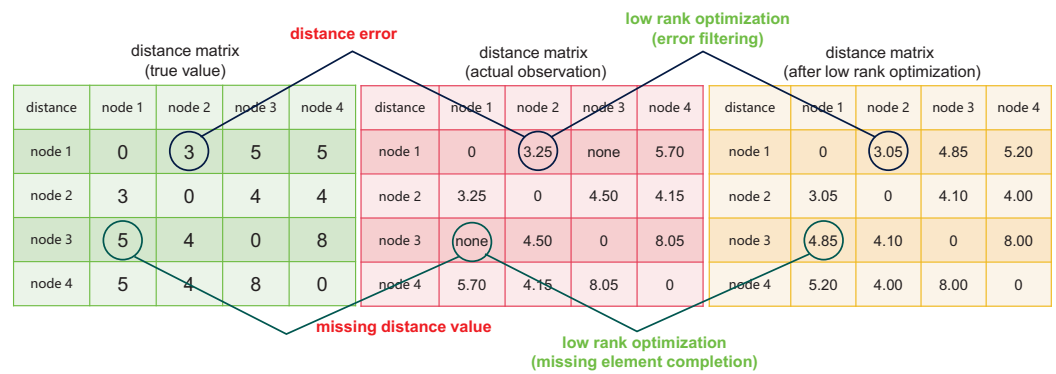


Figure 2. Schematic diagram of low-rank optimization of distance matrix.

### 4.3. Overall Scheme

It is important to note that since the relative positioning algorithm requires aggregating node distance information to a single node for calculation, this approach is not suitable for positioning calculations during high-speed movements of drones. Therefore, this work focuses only on rotary-wing drones, ensuring that they can maintain hovering during relative positioning operations, thus achieving temporal and spatial alignment of distance information.

During the relative positioning operation, the swarm establishes a self-organized connectivity network and then conducts information exchange at different time intervals. For instance, at time  $t_1$ , node 1 transmits a signal, and nodes 2, 3, ...,  $N$  receive the signal and calculate their distances from node 1. At time  $t_i$ , node  $i$  transmits a signal, and the remaining nodes receive the signal and calculate their distances from node  $i$ . Additionally, each node maintains a local distance matrix and shares it with other nodes through the network. Then, all the acquired distance information is aggregated to the master node of the drone swarm, where the ESLO is completed.

In addition, in the case where the electromagnetic environment is too poor to obtain sufficient distance information, the nodes can only temporarily rely on their own navigation equipment for positioning. Additionally, the swarm nodes need to quickly adjust their spatial positions to an open area and wait for improved communication conditions before performing relative positioning.

## 5. Drone Swarm Formation Topology Perception and Relative Positioning

After reconstructing the observation distance matrix through a low-rank optimization algorithm based on eigenvalue scaling, distance errors are effectively filtered out, and missing values are simultaneously completed. At this point, high-precision topology perception and relative positioning calculations can be performed.

In the topology perception calculation of the swarm formation, let  $X$  represent the result of the low-rank optimization of the observation distance matrix. According to the conversion relationship between the distance matrix and the inner product matrix, the inner product matrix  $Q = [q_{ij}]_{N \times N}$  can be calculated as

$$q_{ij} = \frac{1}{2} \left( \frac{1}{N} \sum_{u=1}^N x_{uj}^2 + \frac{1}{N} \sum_{v=1}^N x_{iv}^2 - \frac{1}{N} \sum_{u=1}^N \sum_{v=1}^N x_{uv}^2 - x_{ij}^2 \right) \quad (23)$$

By performing eigenvalue decomposition on  $Q$ , we obtain

$$Q = U \Lambda U^T \quad (24)$$

where  $U$  is the matrix of eigenvectors and  $\Lambda$  is the diagonal matrix of eigenvalues composed of the eigenvalues. By retaining only the first two eigenvalues in  $\Lambda$  and the corresponding eigenvectors in  $U$ , the relative coordinate matrix can be calculated as

$$Y = \Lambda^{\frac{1}{2}} U^T \quad (25)$$

The drone swarm formation performs spatial topology perception based on ranging values, enabling the establishment of a relative coordinate system with the origin of the coordinates set at the centroid of the swarm formation. Topology perception also maps the position of each node into the relative coordinate system, establishing the spatial positional relationship between nodes, as illustrated in the figure below.

After completing topology perception, when the absolute coordinates of some nodes in the swarm formation are known, the transformation relationship between the relative coordinate system and the absolute coordinate system can be calculated, allowing the inference of the absolute coordinates of all nodes and completing the relative positioning calculation. In summary, the overall computational flow of topology perception and relative positioning for the drone swarm formation based on low-rank optimization is as follows in Algorithm 1, and the corresponding calculation results are shown in Figure 3.

---

**Algorithm 1** Topology Perception and Relative Positioning for Drone Swarm Formation Based on Low-rank Optimization

---

**Input:** observation distance matrix  $O$ , eigenvalue scaling threshold  $\mu$ , iteration step  $\epsilon$ , iteration count  $\zeta$

**Output:** relative coordinate  $Y_{2 \times N}$ , absolute coordinate  $H$

**Require:**  $\lambda_{(0)} = 0$ ,  $X_{(0)} = 0$ ; iteration count  $t = 1$

- 1: **while** not converged **do**
  - 2:   Eigenvalue decomposition on  $\lambda_{(k)}$
  - 3:   Scale eigenvalues using the function  $h(\cdot)$
  - 4:   Calculate  $X_{(k+1)}$  according to Equation (21)
  - 5:   Calculate  $\lambda_{(k+1)}$  according to Equation (22)
  - 6:   **if**  $t > \zeta$  **then**
  - 7:     Break
  - 8:   **else**
  - 9:      $t = t + 1$
  - 10:   **end if**
  - 11: **end while**
  - 12: Calculate the inner product matrix  $B$
  - 13: Eigenvalue decomposition on  $B$
  - 14: Retain only the first two eigenvalues of  $B$  and corresponding eigenvectors of  $U$
  - 15: Solve for the relative coordinate  $Y$  according to Equation (25)
  - 16: Calculate transformation relationship between relative and absolute coordinate system
  - 17: Infer the absolute coordinates  $H$  of all UAV nodes
-

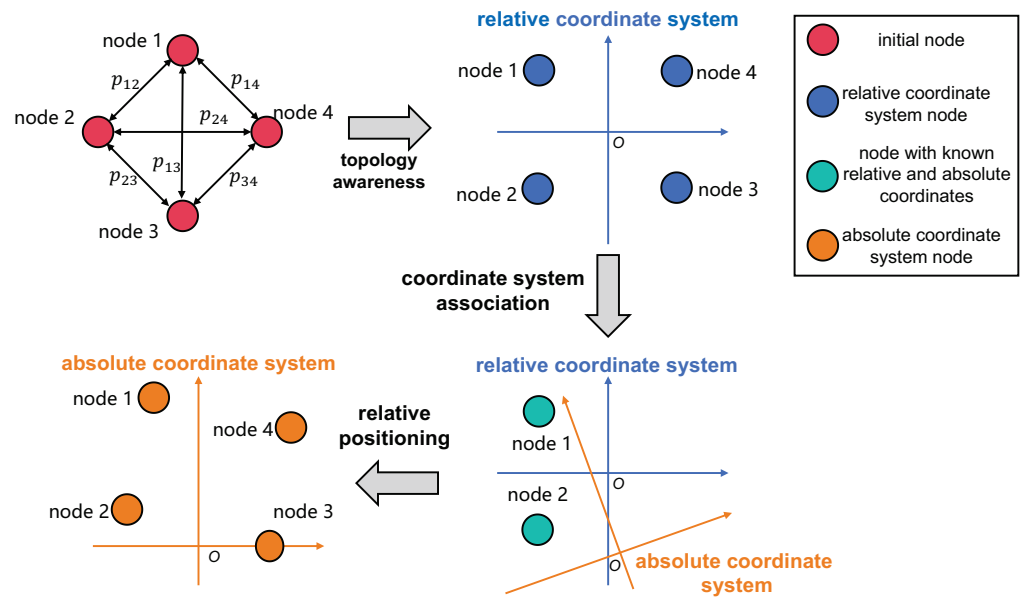


Figure 3. Effect of algorithm calculation result.

### 6. Experiments

To validate the performance of the low-rank optimization-based topology perception and relative positioning algorithm for drone swarm formations, it is necessary to establish a simulation experimental environment. Eight drone nodes in the swarm are randomly distributed within a  $20 \times 20 \text{ km}^2$  area, and their true coordinate values are recorded as  $r_i$ . The true distance matrix between the swarm nodes is designated as  $P$ . For the purpose of relative positioning, the absolute coordinates of three nodes are randomly designated as known. To simulate distance errors and missing distance elements, random Gaussian distance errors and random masks of partial elements can be applied. The distance errors are Gaussian random variables with a mean of zero, and their standard deviation characterizes the intensity of the distance errors.

The evaluation of the algorithm’s performance in the simulation experiments primarily focuses on two aspects: the relative deviation degree of the true value  $\Delta$  and the relative positioning error  $\beta$ . The relative deviation degree of the true value  $\Delta$  is calculated as follows:

$$\Delta = \frac{|X - P|_F}{|P|_F} \times 100\% \tag{26}$$

It is evident that a smaller  $\Delta$  suggests a smaller numerical difference between  $X$  and the true value  $P$ , indicating a better effect of low-rank optimization. The relative positioning error  $\beta$ , is calculated as

$$\beta = \frac{1}{N} \sum_{i=1}^N \left[ (r_i - z_i)^T (r_i - z_i) \right]^{\frac{1}{2}} \tag{27}$$

Here,  $z_i$  represents the calculated node coordinates. A smaller  $\beta$  suggests that  $r_i$  and  $z_i$  are closer, indicating more accurate positioning calculations. In addition, as mentioned above, most current studies directly perform positioning calculations based on raw distance information, and there are currently no relevant distance information optimization methods like ESLO. Therefore, this paper directly compares the performance with relative positioning methods that do not incorporate low-rank optimization.

#### 6.1. Hyperparameter Optimization for ESLO

The ESLO algorithm proposed in this paper incorporates two crucial hyperparameters: the iterative step size  $\epsilon$  and the eigenvalue scaling threshold  $\mu$ . These hyperparameters



have a significant impact on the algorithm's performance and require optimization experiments to ensure its effectiveness. With the distance error intensity set to 10 m and the mask rate set to 20%, experiments are conducted to test different combinations of superparameters. The eigenvalue scaling threshold  $\mu$  is varied from  $10^1$  to  $10^7$  with a gradient setting, with each parameter spaced by an order of magnitude. The iterative step size  $\epsilon$  is set to gradient values of  $10^{-2}$ ,  $10^{-1}$ , 0.5, 1, and 2. The evaluation metric used for these tests is the relative deviation degree of the true value  $\Delta$ , and the results are presented in Table 1 below.

**Table 1.** The influence of iteration step size and eigenvalue compression amplitude for ESLO.

$\Delta$ (%)	$10^1$	$10^2$	$10^3$	$10^4$	$10^5$	$10^6$	$10^7$
$10^{-2}$	11.28	2.36	2.70	1.67	42.32	67.85	89.35
$10^{-1}$	11.18	2.34	0.26	0.27	0.64	57.33	73.22
0.5	10.58	2.35	0.25	0.25	0.31	2.23	68.68
1	11.38	2.27	0.25	0.26	0.27	0.62	47.71
2	89.08	48.15	13.60	13.01	4.08	4.36	7.10

Experimental data indicate that a distance error intensity of 10 m and a random 20% element missingness naturally result in a 12.90% relative deviation of the true value. When using the rank-reduction optimization algorithm with  $(\epsilon, \mu)$  set to  $(10^{-2}, 10^7)$ , the relative deviation of the true value reaches 89.35%, indicating that the algorithm is completely ineffective. However, when  $(\epsilon, \mu)$  is set to  $(10^{-1}, 10^1)$ , the relative deviation of the true value is reduced to 11.18%, suggesting that the low-rank optimization algorithm has achieved a certain level of error filtering and completion. Furthermore, when  $(\epsilon, \mu)$  is set to  $(1, 10^3)$ , the low-rank optimization algorithm nearly achieves complete error filtering for the matrix and accurately complements missing elements, resulting in a relative deviation of the true value of only 0.25%.

Analyzing the trends in the data from Table 1, it can be observed that for a given iterative step size, as the eigenvalue scaling threshold increases by orders of magnitude, the relative deviation of the true value first decreases and then increases. Similarly, for a given eigenvalue scaling threshold, the relative deviation of the true value also first decreases and then increases with the increase in the iterative step size. This suggests that there exists a range of values for  $(\epsilon, \mu)$  that optimizes the performance of the ESLO. In the experimental settings described above, the algorithm achieves optimal performance when the iterative step size  $\epsilon$  falls within the range of  $[10^{-1}, 1]$ , and  $\mu$  falls within the range of  $[10^3, 10^5]$ .

With the optimized parameters, the experiment can proceed to test and verify the algorithm's error filtering capabilities, missing distance element complementation abilities, and overall optimization performance separately.

## 6.2. Error Filtering Capability

During the verification of the algorithm's error filtering performance, the element missingness in the distance matrix (mask rate of 0%) is not considered, and only Gaussian errors are applied to the distance errors. The experiment controls the error intensity by adjusting the standard deviation of the distance errors, with values ranging from 5 m to 100 m with a gradient interval of 5 m. Each error intensity level is tested 50 times, and the average values are taken for analysis. The evaluation metrics include the relative deviation degree of the true distance matrix value and the relative positioning error. The results are presented in Figure 4.

The experimental results demonstrate that the low-rank optimization algorithm for UAV drone swarm formation distance matrices based on eigenvalue scaling can effectively reduce the relative deviation degree of the true value and the relative positioning error. The reduction magnitude is correlated with the intensity of the distance errors. When the distance error intensity is 5 m, the relative deviation degree of the true value without low-rank optimization is 0.18%, and the relative positioning error is 15.54 m. After applying

low-rank optimization, the relative deviation degree of the true value decreases to 0.05%, representing a reduction of 0.13%, while the relative positioning error decreases to 8.32 m, a reduction of 7.22 m. On the other hand, when the distance error intensity is 100 m, the relative deviation degree of the true value without low-rank optimization is 3.78%, and the relative positioning error is 272.40 m. After applying low-rank optimization, the relative deviation degree of the true value decreases to 2.31%, a reduction of 1.47%, and the relative positioning error decreases to 182.50 m, a reduction of 89.90 m.

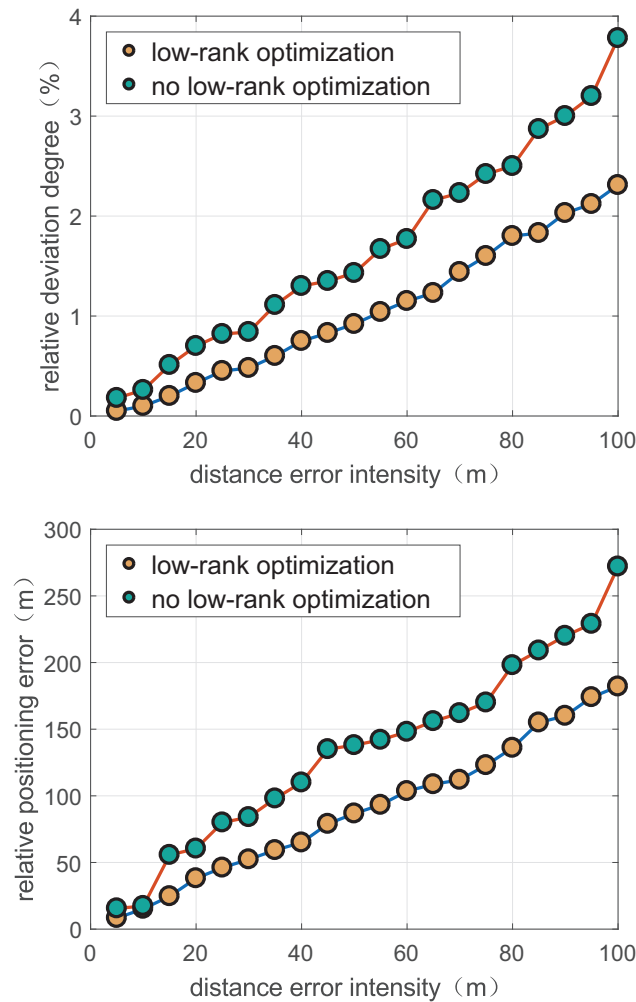


**Figure 4.** Low-rank optimization algorithm error reduction ability.

These results clearly indicate that the low-rank optimization algorithm filters out errors effectively and improves the accuracy of positioning measurements, especially under conditions of high distance error intensity.

### 6.3. Missing Element Completion Capability

In the experiment on the missing distance element completion ability of the algorithm, we do not consider distance errors in the distance matrix but only focus on the situation of partial element missingness. The mask rate is set in a gradient manner from 5% to 95% with an interval of 5% between each level. For each mask rate, 50 experiments are conducted, and the average values are taken for analysis. The evaluation metrics also include the relative deviation degree of the true value and the relative positioning error. The results are presented in Figure 5.

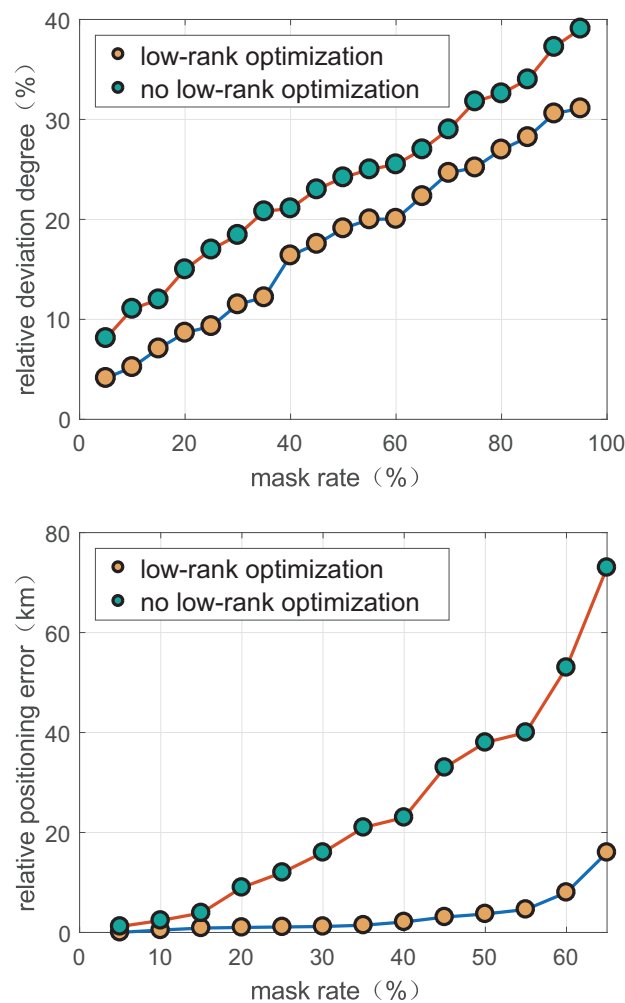


**Figure 5.** Low-rank optimization algorithm missing element completion capability.

The experimental results demonstrate that when the mask rate is 5%, the relative deviation degree of the true value is 8.12%, which is reduced to 4.13% through low-rank optimization. At a mask rate of 95%, the relative deviation degree of the true value is 39.08%, which is reduced to 31.10% with low-rank optimization. Regarding the relative positioning error, when the mask rate reaches 15%, the positioning error without optimization reaches 3.53 km. Although the relative deviation degree of the true value is numerically only 12.02% at this point, the excessively large positioning error can be directly judged as a failure of relative positioning calculation. However, with low-rank optimization, the positioning error is reduced to 0.54 km, still providing a basically accurate spatial position. On the other hand, when the mask rate reaches a high value and there are too many missing elements in the distance matrix, the low-rank optimization algorithm is unable to provide an approximate estimation for the missing elements. For instance, at a mask rate of 45%, the low-rank optimization algorithm produces a positioning error of 3.08 km. When the masking rate is high, there is a significant lack of distance information, resulting in the positioning numerical results being randomly distributed based on factors such as the initial value of iteration and the number of iterations. Therefore, these results do not possess actual physical significance.

In summary, the low-rank optimization method computes and completes missing elements, bringing the calculated distance matrix closer to the true value. More importantly, the algorithm ensures that the observed distance matrix maintains a low-rank property as much as possible, which better aligns with the inherent characteristics of the distance matrix.

#### 6.4. Integrated Optimization Capability

In the comparison experiment on integrated optimization capability, both distance errors and missing element values are taken into account. The performance of the low-rank optimization method is contrasted with the unoptimized approach based on multiple factors: iterative process, the relative deviation degree of distance matrix true value, relative positioning error, and computation time. The experiment involves a total of eight nodes, with the absolute positions of three nodes known. The distance error intensity is set to 10 m, and the mask rate is 20%. The iterative step size  $\epsilon$  of the optimization algorithm is set to 1, and the eigenvalue scaling threshold  $\mu$  is  $10^3$ . The iterative process of the low-rank optimization algorithm is shown in Figure 6.

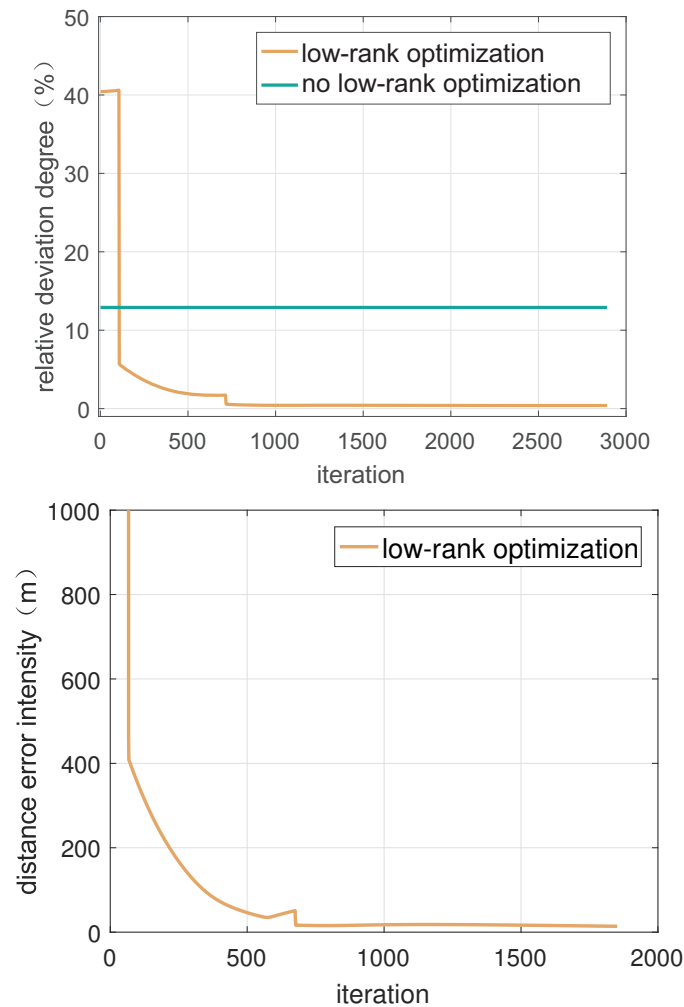


**Figure 6.** Distance matrix relative deviation degree and relative positioning error to iteration.

The unoptimized distance matrix exhibits a relative deviation degree of 11.18% from the true value, with a relative positioning error of 518.05 m. Because of the relatively large setting of the eigenvalue scaling threshold parameter, the optimization algorithm experiences excessively large relative deviation degrees and relative positioning errors during the initial iterations, rendering the relative positioning solution ineffective. However, as the number of iterations reaches around 50 to 500, both the relative deviation degree and the relative positioning error rapidly decrease to lower levels and maintain a convergent state, with values of 0.25% and 35.24 m, respectively. The converged distance matrix exhibits minor differences from the true value, resulting in higher precision in relative positioning solutions, as shown in Figure 7.

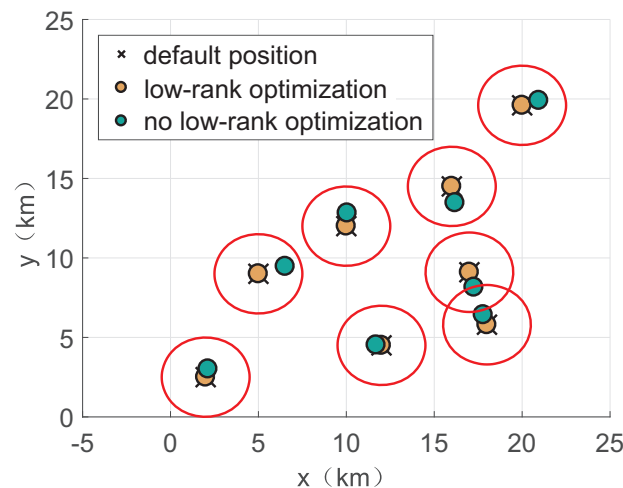


**Figure 7.** Low-rank optimization relative positioning node distribution map.

In terms of computation time, the simulation experiments were conducted using an AMD Ryzen 7 CPU with Matlab 2022 running on a Windows 10 operating system. The single-iteration time for unoptimized relative positioning was 4.05 milliseconds. The total computation time for low-rank optimization relative positioning was 205.14 milliseconds, with 3.02 milliseconds spent on relative positioning calculations. The eigenvalue scaling-based low-rank optimization algorithm for clustered formation distance matrices consumed a total of 202.12 milliseconds, completing 500 iterations with an average of 0.41 milliseconds per iteration. Analysis reveals that the main computational time was occupied by the singular value decomposition of the distance matrix in each iteration step of the low-rank optimization, with a complexity of  $O(N^3)$ .

## 7. Discussion

The UAV swarm formation, leveraging low-rank optimization through the eigenvalue shrinkage low-rank optimization (ESLO) algorithm, enables the observed distance matrix to converge toward the true value. This approach enhances the precision of topological perception and reduces the relative positioning error within the swarm. Simulation experiments demonstrate that the performance of the algorithm is closely related to two parameters: the iterative step size and the eigenvalue scaling threshold. Furthermore, there exists an optimal parameter range that minimizes both the relative deviation degree from the true value and the relative positioning error.

Error filtering experiments reveal that the algorithm possesses the ability to filter out distance errors, and this capability becomes more pronounced in scenarios with high distance error intensities. The missing element completion experiments show that, in cases where some elements of the distance matrix are missing, the algorithm can approximate the missing values, thereby reducing the positioning error. However, when the degree of missing elements exceeds a certain threshold, the algorithm becomes unable to perform effective relative positioning calculations.

Finally, comprehensive experiments considering both distance error and distance missing elements indicate that, during the iterative optimization process, the algorithm gradually reduces the relative deviation degree from the true value and the relative positioning error. It converges to a neighborhood close to the true value of the distance matrix. Our algorithm significantly reduces the relative positioning error, effectively enhancing the robustness of the relative positioning algorithm and strengthening the survival and operational capabilities of the UAV swarm formation.

## 8. Conclusions

With the rapid development and widespread application of drone technology, the field of relative positioning for UAV swarm formations is poised to present even richer research content and broader application prospects. On the one hand, ranging accuracy is a core factor that significantly impacts relative positioning. Therefore, further research is required in the area of data link technology for UAV swarm formations, aiming to enhance the distance and angle measurement capabilities of the data link. Additionally, there is a need to explore relative positioning methods that can comprehensively utilize both distance and angle measurement information.

On the other hand, there is a need to integrate relative positioning navigation functions with communication capabilities, enabling a unified design of hardware and software for both communication and navigation. This approach can help reduce costs and energy consumption, while simultaneously enhancing the swarm's collaborative capabilities, mission execution efficiency, and overall system robustness.

**Author Contributions:** Conceptualization, C.D.; methodology, C.D.; software, X.G.; formal analysis, X.G.; investigation, C.D.; resources, X.G.; data curation, X.G.; writing—original draft preparation, C.D.; writing—review and editing, X.G.; visualization, X.G.; supervision, C.D. All authors have read and agreed to the published version of the manuscript.

**Funding:** This research was funded by National Natural Science Foundation: Semantic Situation Construction of Unmanned Battlefield Based on Multi source Heterogeneous Image Analysis, grant number is 62101517.

**Data Availability Statement:** The data are available from the corresponding author on reasonable request.

**Conflicts of Interest:** No potential conflict of interest was reported by the authors.

## References

1. Ma'Sum, M.A.; Arrofi, M.K.; Jati, G.; Arifin, F.; Kurniawan, M.N.; Mursanto, P.; Jatmiko, W. Simulation of intelligent unmanned aerial vehicle (UAV) for military surveillance. In Proceedings of the 2013 International Conference on Advanced Computer Science and Information Systems (ICACSIS), Sanur Bali, Indonesia, 28–29 September 2013; IEEE: Piscataway, NJ, USA, 2013; pp. 161–166.
2. Christensen, C.; Salmon, J. An agent-based modeling approach for simulating the impact of small unmanned aircraft systems on future battlefields. *J. Def. Model. Simul.* **2022**, *19*, 481–500. [[CrossRef](#)]
3. Xiaoning, Z. Analysis of military application of UAV swarm technology. In Proceedings of the 2020 3rd International Conference on Unmanned Systems (ICUS), Harbin, China, 27–28 November 2020; IEEE: Piscataway, NJ, USA, 2020; pp. 1200–1204.
4. Kritsky, D.; Ovsianik, V.; Pogudina, O.; Shevel, V.; Druzhinin, E. Model for intercepting targets by the unmanned aerial vehicle. In Proceedings of the International Scientific-Practical Conference, Chernihiv, Ukraine, 24–26 June 2019; Springer: Berlin/Heidelberg, Germany, 2019; pp. 197–206.
5. Pinkney, M.F.; Hampel, D.; DiPierro, S. Unmanned aerial vehicle (UAV) communications relay. In Proceedings of the MILCOM'96 IEEE Military Communications Conference, McLean, VA, USA, 24 October 1996; IEEE: Piscataway, NJ, USA, 1996; Volume 1; pp. 47–51.
6. Champion, M.; Ranganathan, P.; Faruque, S. UAV swarm communication and control architectures: A review. *J. Unmanned Veh. Syst.* **2018**, *7*, 93–106. [[CrossRef](#)]
7. Guitton, M.J. Fighting the locusts: Implementing military countermeasures against drones and drone swarms. *Scand. J. Mil. Stud.* **2021**, *4*, 26–36. [[CrossRef](#)]
8. He, D.; Yang, G.; Li, H.; Chan, S.; Cheng, Y.; Guizani, N. An effective countermeasure against UAV swarm attack. *IEEE Netw.* **2020**, *35*, 380–385. [[CrossRef](#)]
9. Cevik, P.; Kocaman, I.; Akgul, A.S.; Akca, B. The small and silent force multiplier: A swarm UAV—Electronic attack. *J. Intell. Robot. Syst.* **2013**, *70*, 595–608. [[CrossRef](#)]
10. Tianfeng, F.; Xiaojing, M.; Chi, Z. Development status of anti UAV swarm and analysis of new defense system. *J. Phys. Conf. Ser.* **2023**, *2478*, 092011. [[CrossRef](#)]
11. Gaydamaka, A.; Samuylov, A.; Moltchanov, D.; Ashraf, M.; Tan, B.; Koucheryavy, Y. Dynamic Topology Organization and Maintenance Algorithms for Autonomous UAV Swarms. *IEEE Trans. Mob. Comput.* **2023**, *23*, 4423–4439. [[CrossRef](#)]
12. Mykytyn, P.; Brzozowski, M.; Dyka, Z.; Langendoerfer, P. GPS-spoofing attack detection mechanism for UAV swarms. In Proceedings of the 2023 12th Mediterranean Conference on Embedded Computing (MECO), Budva, Montenegro, 6–10 June 2023; IEEE: Piscataway, NJ, USA, 2023; pp. 1–8.



13. Qiao, X.; Cong, Y.; Wang, K.; Wang, X. UAV Path Replanning Based on BeiDou Short Message Communication Function. In Proceedings of the 2023 42nd Chinese Control Conference (CCC), Tianjin, China, 24–26 July; IEEE: Piscataway, NJ, USA, 2023; pp. 2904–2909.
14. Wang, H.; Zhang, Y.; Shen, Y.; Zhu, J.; Chen, Y.; Jiang, X. Novel Replay Attacks Against Galileo Open Service Navigation Message Authentication. In Proceedings of the 36th International Technical Meeting of the Satellite Division of The Institute of Navigation (ION GNSS+ 2023), Denver, CO, USA, 11–15 September 2023; pp. 3897–3907.
15. Du, S.; Xu, M.; Liu, M.; Zhang, G.; Xia, S.; Liu, Q. Resonant Beam Enabled Relative Localization for UAV Swarm. *IEEE Internet Things J.* **2024**, *11*, 17827–17839. [[CrossRef](#)]
16. Uspenskyi, V.B.; Shyriaieva, N.V. Relative navigation of UAV in a swarm. In Proceedings of the 2023 IEEE 4th KhPI Week on Advanced Technology (KhPIWeek), Kharkiv, Ukraine, 2–6 October 2023; IEEE: Piscataway, NJ, USA, 2023; pp. 1–5.
17. Tong, P.; Yang, X.; Yang, Y.; Liu, W.; Wu, P. Multi-UAV collaborative absolute vision positioning and navigation: A survey and discussion. *Drones* **2023**, *7*, 261. [[CrossRef](#)]
18. Zhang, Z.; Zhou, Y.; Zhang, Y.; Qian, B. Strong Electromagnetic Interference and Protection in UAVs. *Electronics* **2024**, *13*, 393. [[CrossRef](#)]
19. Ren, M.; Wang, B.; Guo, Q. Electromagnetic Segmentation Technology for Heterogeneous Unmanned Aerial Vehicles Based on Mosaic Warfare. In Proceedings of the China Conference on Command and Control, Beijing, China, 24–25 October 2023; Springer: Berlin/Heidelberg, Germany, 2023; pp. 109–115.
20. Zhu, Q.; Liu, R.; Wang, Z.; Liu, Q.; Chen, C. Sensing-Communication Co-Design for UAV Swarm-Assisted Vehicular Network in Perspective of Doppler. *IEEE Trans. Veh. Technol.* **2023**, *73*, 2578–2592. [[CrossRef](#)]
21. Boiteau, S.; Vanegas, F.; Gonzalez, F. Framework for Autonomous UAV Navigation and Target Detection in Global-Navigation-Satellite-System-Denied and Visually Degraded Environments. *Remote Sens.* **2024**, *16*, 471. [[CrossRef](#)]
22. Lou, T.s.; Chen, N.; Jiao, Y.; Zhao, H.; Zhao, L. A consider unscented particle filter with genetic algorithm for UAV multi-source integrated navigation. *Meas. Sci. Technol.* **2023**, *34*, 095105. [[CrossRef](#)]
23. Iyer, K.; Dey, A.; Xu, B.; Sharma, N.; Hsu, L.T. Enhancing Positioning in GNSS Denied Environments based on an Extended Kalman Filter Using Past GNSS Measurements and IMU. *IEEE Trans. Veh. Technol.* **2024**, *99*, 1–16. [[CrossRef](#)]
24. Cheng, J.; Ren, P.; Deng, T. A Novel Ranging and IMU-Based Method for Relative Positioning of Two-MAV Formation in GNSS-Denied Environments. *Sensors* **2023**, *23*, 4366. [[CrossRef](#)] [[PubMed](#)]
25. Hao, W.; Zhonghong, W.; Zhangsong, S.; Shiyan, S.; Pengfei, W.; Zhi, W. Swarm intelligence based clustering and localizing methods for loitering munitions in a satellite denied environment. *Chin. J. Aeronaut.* **2023**, *36*, 409–433.
26. Karagüzel, T.A.; Turgut, A.E.; Eiben, A.; Ferrante, E. Collective gradient perception with a flying robot swarm. *Swarm Intell.* **2023**, *17*, 117–146. [[CrossRef](#)]
27. Pengfei, W.; Jinfeng, H.; Wen, H.; Weiguang, W.; Hao, D. Anti-swarm UAV radar system based on detection data fusion. *J. Syst. Eng. Electron.* **2023**, *99*, 1–10. [[CrossRef](#)]
28. Chen, W.; Zhu, J.; Liu, J.; Guo, H. A fast coordination approach for large-scale drone swarm. *J. Netw. Comput. Appl.* **2024**, *221*, 103769. [[CrossRef](#)]
29. Tang, J.; Duan, H.; Lao, S. Swarm intelligence algorithms for multiple unmanned aerial vehicles collaboration: A comprehensive review. *Artif. Intell. Rev.* **2023**, *56*, 4295–4327. [[CrossRef](#)]
30. Park, J.S.; Song, Y.H.; Lee, B.H.; Yoon, C.B. A study on position estimation for UAV using line-of-sight data-link system. *J. Korea Inst. Electron. Commun. Sci.* **2016**, *11*, 1031–1038. [[CrossRef](#)]
31. Luo, C.; McClean, S.I.; Parr, G.; Teacy, L.; De Nardi, R. UAV position estimation and collision avoidance using the extended Kalman filter. *IEEE Trans. Veh. Technol.* **2013**, *62*, 2749–2762. [[CrossRef](#)]
32. Balamurugan, G.; Valarmathi, J.; Naidu, V. Survey on UAV navigation in GPS denied environments. In Proceedings of the 2016 International Conference on Signal Processing, Communication, Power and Embedded System (SCOPES), Paralakhemundi, India, 3–5 October 2016; IEEE: Piscataway, NJ, USA, 2016; pp. 198–204.
33. Zhu, X.; Lai, J.; Chen, S. Cooperative Location Method for Leader-Follower UAV Formation Based on Follower UAV's Moving Vector. *Sensors* **2022**, *22*, 7125. [[CrossRef](#)] [[PubMed](#)]
34. Zhang, D.; Duan, H.; Zeng, Z. Leader-follower interactive potential for target enclosing of perception-limited UAV groups. *IEEE Syst. J.* **2021**, *16*, 856–867. [[CrossRef](#)]
35. Li, J.; Zhou, Y.; Lamont, L. Communication architectures and protocols for networking unmanned aerial vehicles. In Proceedings of the 2013 IEEE Globecom Workshops (GC Wkshps), Atlanta, GA, USA, 9–13 December 2013; IEEE: Piscataway, NJ, USA, 2013; pp. 1415–1420.
36. Koushik, A.; Hu, F.; Kumar, S. Deep Q-learning-based node positioning for throughput-optimal communications in dynamic UAV swarm network. *IEEE Trans. Cogn. Commun. Netw.* **2019**, *5*, 554–566. [[CrossRef](#)]
37. Liu, Y.; Wang, Y.; Shen, X.; Wang, J.; Shen, Y. UAV-aided relative localization of terminals. *IEEE Internet Things J.* **2021**, *8*, 12999–13013. [[CrossRef](#)]
38. Li, Z.; Yin, D.; Xiang, X.; Tang, D.; Zhang, C.; Zhang, S. Research on relative positioning system of UAVs Swarm based on distributed UWB. In Proceedings of the 2020 Chinese Automation Congress (CAC), Shanghai, China, 6–8 November 2020; IEEE: Piscataway, NJ, USA, 2020; pp. 5561–5566.

39. Wang, Z.; Sun, H.; Li, H.; Lai, T. AOA Positioning and Path Optimization of UAV Swarm Based on A-Optimality. *IEEE Access* **2022**, *10*, 14946–14958. [[CrossRef](#)]
40. Chen, S.; Yin, D.; Niu, Y. A survey of robot swarms' relative localization method. *Sensors* **2022**, *22*, 4424. [[CrossRef](#)]
41. Chen, R.; Yang, B.; Zhang, W. Distributed and collaborative localization for swarming UAVs. *IEEE Internet Things J.* **2020**, *8*, 5062–5074. [[CrossRef](#)]

**Disclaimer/Publisher's Note:** The statements, opinions and data contained in all publications are solely those of the individual author(s) and contributor(s) and not of MDPI and/or the editor(s). MDPI and/or the editor(s) disclaim responsibility for any injury to people or property resulting from any ideas, methods, instructions or products referred to in the content.